Journal of Organometallic Chemistry 695 (2010) 2726–2731

Contents lists available at ScienceDirect

Journal of Organometallic Chemistry

journal homepage: www.elsevier.com/locate/jorganchem

Synthesis and characterization of lanthanide complexes bearing a ferrocene-containing N-aryloxo-β-ketoiminate ligand

Xiang-Yong Gu, Xiang-Zong Han, Ying-Ming Yao*, Yong Zhang, Qi Shen

Key Laboratory of Organic Synthesis of Jiangsu Province, College of Chemistry, Chemical Engineering & Materials Science, Dushu Lake Campus, Soochow University, Suzhou 215123, PR China

ARTICLE INFO

Article history:
Received 30 April 2010
Received in revised form
20 July 2010
Accepted 30 July 2010
Available online 7 August 2010

Keywords:
Organolanthanides
β-Ketoiminate ligand
Synthesis
Crystal structure
Polymerization
L-Lactide

ABSTRACT

A series of organolanthanide complexes supported by a new ferrocene-containing N-aryloxo-functionalized β-ketoiminate ligand $FcCOCH_2C(Me)N(2\text{-}HO\text{-}5\text{-}Me\text{-}C_6H_3)$ (LH_2, Fc = ferrocenyl) was synthesized by amine elimination reactions. It was found that the ionic radii have a profound effect on the outcome of the reactions. Reactions of LH_2 with $Ln[N(SiMe_3)_2]_3(\mu\text{-}Cl)Li(THF)_3$ in a 1:1 molar ratio in THF gave the desired lanthanide amido complexes $[LLn\{N(SiMe_3)_2\}(THF)]_2$ [Ln = Nd (**1**), Sm (**2**), Er (**3**), Yb (**4**), Y (**5**)] in good isolated yields, whereas the similar reaction of LH_2 with $La[N(SiMe_3)_2]_3(\mu\text{-}Cl)Li(THF)_3$ gave the unexpected lanthanum–lithium heterobimetallic cluster $[L_2La\{\mu\text{-}Li(THF)\}_2(\mu\text{-}Cl)]_2$ (**6**). These complexes were characterized by IR spectroscopy, elemental analysis, and ^1H NMR spectroscopy in the case of complexes **5** and **6**. The definitive molecular structures of complexes **1**, **2**, **4** and **6** were determined by X-ray diffraction studies. Complexes **1**–**5** can initiate the ring-opening polymerization of L-lactide with moderate activity.

1. Introduction

Over the past decades, significant efforts to explore ligands other than the traditional ancillary ligand bis(cyclopentadienyl) set in organometallic lanthanide chemistry have led to the fruitful design of new non-cyclopentadienyl ligand systems to stabilize a series of organolanthanide complexes [1–3]. Of these new alternatives, nitrogen-containing ligands, such as guanidinate, amidinate [4], β-diketiminate [5] and bridged bisamide [6] ligands have received much attention, because their electronic properties and steric bulkiness can be easily modified by variation of the substituents on the nitrogen atoms. β-Ketoiminate ligand, as one kind of nitrogen-containing ligands, have become among the most attractive chelating systems in main group and transition metal coordination chemistry. These metal complexes have been used in various applications, such as precursors for metal–organic chemical vapor deposition (MOCVD) for the growth of thin films [7], and as active catalysts in homogeneous catalysis [8–11]. However, these ligands have seldom been used in organolanthanide chemistry, and only a few lanthanide complexes stabilized by β-ketoiminate ligands have been reported [12–14].

Recently, we became interested in studying the synthesis and reactivity of organolanthanide complexes supported by N-aryloxo-functionalized β-ketoiminate ligands. In our earlier work, a series of new lanthanide chlorides and aryloxides based on this ligand were synthesized and it was found that the corresponding lanthanide aryloxides are active initiators for the ring-opening polymerization of L-lactide [15]. These results indicated that the dianionic functionalized β-ketoiminate ligands might have potential in the design and synthesis of organolanthanide catalysts for homogeneous catalysis. However, the catalytic activity of these lanthanide complexes is relatively low in comparison with other organolanthanide initiators, which was attributed to the formation of stable dimeric structures via the bridging phenoxo oxygen atoms. So we intend to introduce a bulky substituent to the ligand, and try to synthesize monomeric organolanthaide complexes. In this contribution, a new ferrocene-containing N-aryloxo-functionalized β-ketoiminate ligand $FcCOCH_2C(Me)N(2\text{-}HO\text{-}5\text{-}Me\text{-}C_6H_3)$ (LH_2, Fc = ferrocenyl) was synthesized, and some organolanthanide complexes stabilized by this ligand were prepared via amine elimination reactions. It was found that the ionic radii have a profound effect on the outcome of the reactions. Here we report these results.

* Corresponding author. Soochow University, College of Chemistry, Chemical Engineering & Materials Science, Dushu Lake Campus, Suzhou, 215123, PR China. Tel.: +86 512 65882806; fax: +86 512 65880305.
E-mail address: yaoym@suda.edu.cn (Y.-M. Yao).

0022-328X/$ – see front matter © 2010 Elsevier B.V. All rights reserved.
doi:10.1016/j.jorganchem.2010.07.037

2. Experimental Section

The complexes described below are extremely sensitive to air and moisture. Therefore, all manipulations were performed under pure argon with rigorous exclusion of air and moisture using Schlenk techniques. Solvents were dried and freed of oxygen by refluxing over sodium/benzophenone ketyl and distilled prior to use. Ferrocenoylacetone [16] and $Ln[N(TMS)_2]_3(\mu\text{-}Cl)Li(THF)_3$ (Ln = La, Nd, Sm, Er, Yb, Y) [17] were prepared according to the literature procedures. L-Lactide was purchased from Arcos, and was recrystallized from hot anhydrous toluene twice. The uncorrected melting points of crystalline samples in sealed capillaries (under argon) are reported as ranges. Lanthanide metal analyses were performed by EDTA titration with a xylenol orange indicator and a hexamine buffer [18]. Carbon, hydrogen and nitrogen analyses were performed by direct combustion with a Carlo-Erba EA-1110 instrument. The IR spectra were recorded with a Nicolet-550 FT-IR spectrometer as KBr pellets. The ^1H NMR spectra were recorded in C_6D_6 solution for the yttrium and lanthanum complexes and in $CDCl_3$ solution for the ligand with a Unity Varian-400 spectrometer. Molecular weight and molecular weight distribution (PDI) were determined against polystyrene standards by gel permeation chromatography (GPC) on a PL 50 apparatus, and THF was used as an eluent at a flow rate of 1.0 mL/min at 40 °C.

2.1. Synthesis of LH_2

To a solution of ferrocenoylacetone (27.0 g, 0.10 mol) in absolute ethanol (60 mL) was added 2-amino-4-methyl-phenol (12.3 g, 0.l0 mol) in absolute ethanol (30 mL) dropwise at room temperature. After stirring in oil bath and refluxing for 2 h, the mixture was concentrated to about 25 mL under reduced pressure. Ligand LH_2 was obtained as red–yellow block crystals by filtration in the next day (26.3 g, 70%). Mp: 190–191 °C (dec). Anal. Calc. for $C_{21}H_{21}FeNO_2$: C, 67.22; H, 5.64; N, 3.73. Found: C, 67.11; H, 5.51; N, 4.12. ^1H NMR (400 MHz, $CDCl_3$, 25 °C) 1.78 (s, 3H, $CH_3C{=}N$), 2.26 (s, 3H, CH_3 (arene)), 4.20 (s, 5H, C_5H_5), 4.40 (s, 2H, (H^3, H^4), C_5H_4), 4.74 (s, 2H, (H^2, H^5), C_5H_4), 5.40 (s, 1H, CH), 6.90–7.26 (m, 3H, Ar), 11.76 (s, 1H, PhOH). ^{13}C NMR (400 MHz, $CDCl_3$, 25 °C) 193.06, 162.07, 149.87, 129.33, 128.75, 127.92, 125.36, 116.72, 82.12, 70.96, 69.88, 68.59, 20.41, 20.07. IR (KBr, cm^{-1}): 3411 (s), 3036 (s), 2346 (s), 1591 (s), 1528 (s), 1387 (s), 1289 (s), 1250 (s), 1196 (s), 1057 (m), 887 (m), 803 (s), 679 (m), 567 (w).

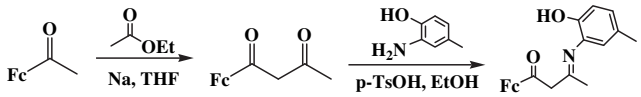

Scheme 1.

2.2. Synthesis of $[LNd\{N(SiMe_3)_2\}(THF)]_2$ (**1**)

A THF solution (20 mL) of $Nd[N(TMS)_2]_3(\mu\text{-}Cl)Li(THF)_3$ (1.05 mmol) was added to a THF solution (20 mL) of LH_2 (0.40 g, 1.05 mmol). The mixture was stirred at room temperature for 20 min, and precipitate formed gradually. The mixture was stirred overnight, and then the precipitate was separated from the solution by centrifugation. The powder was dissolved with hot THF, and red crystals were obtained from a concentrated THF solution (20 mL) at room temperature (0.66 g, 84%). Mp: 192–194 °C (dec). Anal. Calc. for $C_{62}H_{90}Fe_2N_4Nd_2O_6Si_4$: C, 49.65; H, 6.05; N, 3.73; Nd, 19.23. Found: C, 49.27; H, 5.85; N, 4.04; Nd, 19.41. IR (KBr, cm^{-1}): 2954 (s), 1595 (s), 1496 (s), 1409 (s), 1352 (s), 1276 (s), 1126 (m), 1019 (m), 934 (s), 835 (s), 762 (w), 682 (m), 626 (m), 525 (w). Crystals suitable for an X-ray structure analysis were obtained from a concentrated THF solution.

2.3. Synthesis of $[LSm\{N(SiMe_3)_2\}(THF)]_2$ (**2**)

The synthesis of complex **2** was carried out in the same way as that described for complex **1**, but $Sm[N(TMS)_2]_3(\mu\text{-}Cl)Li(THF)_3$ (1.30 mmol) was used instead of $Nd[N(TMS)_2]_3(\mu\text{-}Cl)Li(THF)_3$. Red microcrystals were obtained from a concentrated THF solution at room temperature (0.78 g, 80%). Mp: 197–199 °C (dec). Anal. Calc. for $C_{62}H_{90}Fe_2N_4O_6Si_4Sm_2$: C, 49.25; H, 6.00; N, 3.70; Sm, 19.89.

Table 1
Crystallographic data for complexes 1, 2, 4 and 6.

complex	**1**·2THF	**2**·2THF	**4**·2THF	**6**·3THF
formula	$C_{70}H_{106}Fe_2N_4Nd_2O_8Si_4$	$C_{70}H_{106}Fe_2N_4O_8Si_4Sm_2$	$C_{70}H_{106}Fe_2N_4O_8Si_4Yb_2$	$C_{112}H_{132}Cl_2Fe_4La_2Li_4N_4O_{15}$
fw	1644.13	1656.35	1701.73	2374.10
T(K)	223(2)	223(2)	293(2)	223(2)
crystal system	triclinic	triclinic	triclinic	monoclinic
crystal size (mm)	0.39 × 0.38 × 0.25	0.22 × 0.18 × 0.15	0.50 × 0.40 × 0.40	0.40 × 0.20 × 0.15
space group	$P\bar{1}$	$P\bar{1}$	$P\bar{1}$	$P2_1/n$
a (Å)	11.7480(16)	11.6026(7)	11.4609(3)	15.769(4)
b (Å)	13.4189(17)	13.2790(7)	13.2300(2)	22.348(6)
c (Å)	14.5079(16)	14.4908(7)	14.3545(2)	17.340(5)
α (deg)	62.470(10)	117.246(8)	116.805(3)	
β (deg)	74.232(13)	94.317(11)	93.870(4)	112.279(4)
γ (deg)	77.916(14)	102.320(12)	102.546(4)	
V (Å^3)	1942.4(4)	1900.35(17)	1861.77(6)	5655(3)
Z	1	1	1	2
D_{calcd} (Mg m^{-3})	1.406	1.447	1.518	1.394
μ (mm^{-1})	1.793	2.012	2.988	1.346
F(000)	846	850	866	2432
θ_{max} (deg)	25.35	25.50	25.50	25.50
collected reflns	18838	16497	15145	19581
unique reflns	7062	7031	6881	10337
obsd reflns [$I > 2.0\sigma(I)$]	6101	6170	6506	7867
no. of variables	382	377	377	597
GOF	1.123	1.149	1.070	1.153
R	0.0578	0.0661	0.0387	0.0839
wR	0.1310	0.1488	0.1008	0.1936
largest diff peak, hole (e.Å^{-3})	1.557, −0.859	1.589, −0.944	2.194, −1.286	2.144, −1.216

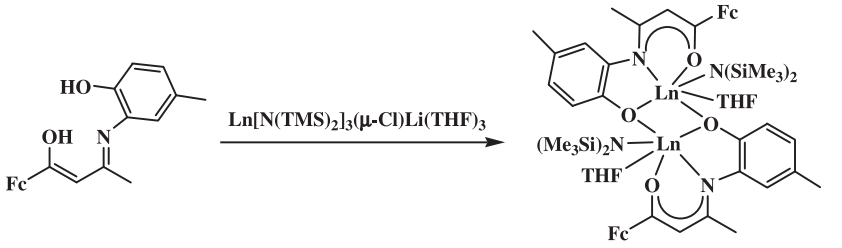

Ln = Nd (1), Sm (2), Er (3), Yb (4), Y (5)

Scheme 2.

Found: C, 49.54; H, 6.21; N, 3.78. Sm, 19.62. IR (KBr, cm^{-1}): 2955 (s), 1590 (s), 1497 (s), 1400 (s), 1349 (s), 1270 (s), 1127 (m), 1021 (m), 933 (s), 850 (s), 756 (w), 680 (m), 527 (w). Crystals suitable for an X-ray structure analysis were obtained from a concentrated THF solution.

2.4. Synthesis of [LEr{N(SiMe$_3$)$_2$}(THF)]$_2$ (**3**)

The synthesis of complex **3** was carried out in the same way as that described for complex **1**, but Er[N(TMS)$_2$]$_3$(μ-Cl)Li(THF)$_3$ (1.22 mmol) was used instead of Nd[N(TMS)$_2$]$_3$(μ-Cl)Li(THF)$_3$. Red microcrystals were obtained from a concentrated THF solution at room temperature (0.71 g, 75%). Mp: 198–200 °C (dec). Anal. Calc. for $C_{62}H_{90}Er_2Fe_2N_4O_6Si_4$: C, 48.17; H, 5.87; N, 3.62; Er, 21.64. Found: C, 47.94; H, 5.51; N, 3.34; Er, 21.27. IR (KBr, cm^{-1}): 2950 (s), 1578 (s), 1485 (s), 1421 (s), 1362 (s), 1271 (s), 1124 (m), 1018 (m), 943 (s), 848 (s), 753 (w), 677 (m), 527 (w).

2.5. Synthesis of [LYb{N(SiMe$_3$)$_2$}(THF)]$_2$ (**4**)

The synthesis of complex **4** was carried out in the same way as that described for complex **1**, but Yb[N(TMS)$_2$]$_3$(μ-Cl)Li(THF)$_3$ (1.17 mmol) was used instead of Nd[N(TMS)$_2$]$_3$(μ-Cl)Li(THF)$_3$. Red microcrystals were obtained from a concentrated THF solution at room temperature (0.64 g, 70%). Mp: 193–195 °C (dec). Anal. Calc. for $C_{62}H_{90}N_4O_6Si_4Fe_2Yb_2$: C, 47.81; H, 5.82; N, 3.60; Yb, 22.22. Found: C, 47.44; H, 5.41; N, 3.78; Yb, 22.40. IR (KBr, cm^{-1}): 2954 (s), 1594 (s), 1499 (s), 1412 (s), 1349 (s), 1266 (s), 1129 (m), 1017 (m), 934 (s), 840 (s), 765 (w), 665 (m), 599 (m), 521 (w). Crystals suitable for an X-ray structure analysis were obtained from a concentrated THF solution.

2.6. Synthesis of [LY{N(SiMe$_3$)$_2$}(THF)]$_2$ (**5**)

The synthesis of complex **5** was carried out in the same way as that described for complex **1**, but Y[N(TMS)$_2$]$_3$(μ-Cl)Li(THF)$_3$ (1.20 mmol) was used instead of Nd[N(TMS)$_2$]$_3$(μ-Cl)Li(THF)$_3$. Red microcrystals were obtained from a concentrated THF solution at room temperature (0.60 g, 72%). Mp: 196–198 °C (dec). Anal. Calc. for $C_{62}H_{90}Fe_2N_4O_6Si_4Y_2$: C, 53.90; H, 7.78; N, 4.03; Y, 12.97. Found: C, 54.25; H, 7.52; N, 3.86; Y, 12.52. ^{1}H NMR (400 MHz, C_6D_6, 25 °C): 0.15 (s, 36H, Si(CH$_3$)$_3$), 1.33 (s, 8H, CH$_2$ of THF), 1.73 (s, 6H, CH$_3$C=N), 2.20 (s, 6H, CH$_3$ (arene)), 3.80 (s, 8H, CH$_2$O of THF), 4.20–4.70 (m, 18H, Cp), 5.60 (s, 2H, CH), 7.12–7.30 (m, 6H, Ar). IR (KBr, cm^{-1}): 2952 (s), 1592 (s), 1488 (s), 1413 (s), 1336 (s), 1264 (s), 1120 (m), 1020 (m), 931 (s), 853 (s), 759 (w), 668 (m), 522 (w).

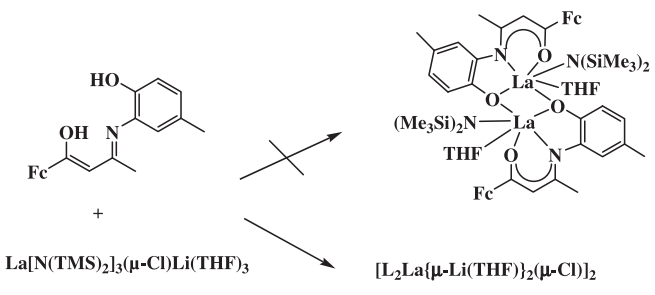

Scheme 3.

2.7. Synthesis of [L$_2$La{μ-Li(THF)}$_2$(μ-Cl)]$_2$ (**6**)

The synthesis of complex **6** was carried out in the same way as that described for complex **1**, but La[N(TMS)$_2$]$_3$(μ-Cl)Li(THF)$_3$ (1.13 mmol) was used instead of Nd[N(TMS)$_2$]$_3$(μ-Cl)Li(THF)$_3$. Red microcrystals were obtained from a concentrated THF solution at room temperature (0.38 g, 31%). Mp: 210 212 °C (dec). Anal. Calc. for $C_{100}H_{108}Cl_2Fe_4La_2Li_4N_4O_{12}$: C, 55.66; H, 5.04; N, 2.60; La, 12.88. Found: C, 56.01; H, 5.06; N, 2.73; La, 13.13. ^{1}H NMR (400 MHz, C_6D_6, 25 °C): 1.38 (s, 16H, CH$_2$ of THF), 1.70 (s, 12H, CH$_3$C=N), 2.15 (s, 12H, CH$_3$ (arene)), 3.54 (s, 16H, CH$_2$O of THF), 3.92–4.14 (m, 36H, Cp), 5.20 (s, 4H, CH), 7.06–7.20 (m, 12H, Ar). IR (KBr, cm^{-1}): 2975 (m), 1739 (s), 1548 (s), 1428 (s), 1358 (s), 1275 (s), 1208 (m), 1121 (m), 1022 (m), 922 (w), 798 (w), 669 (m), 487 (m), 437 (s). Crystals suitable for an X-ray structure analysis were obtained from a concentrated THF solution.

2.8. X-ray crystallography

Suitable single-crystals of complexes **1**, **2**, **4**, and **6** were sealed in a thin-walled glass capillary for determining the single-crystal

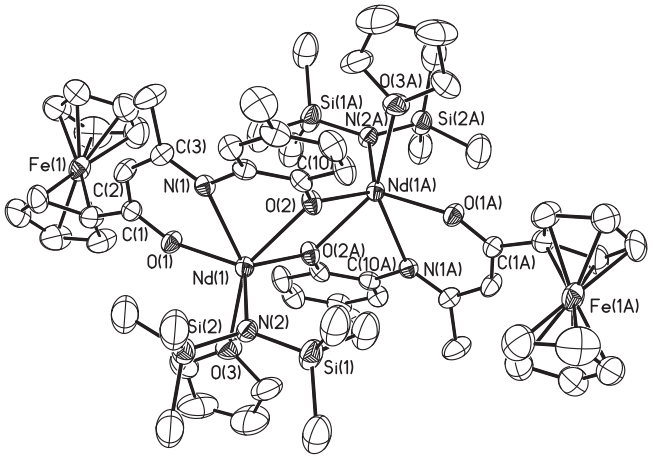

Fig. 1. ORTEP diagram of complex **1** showing atom-numbering scheme. Thermal ellipsoids are drawn at the 20% probability level. Hydrogen atoms are omitted for clarity.

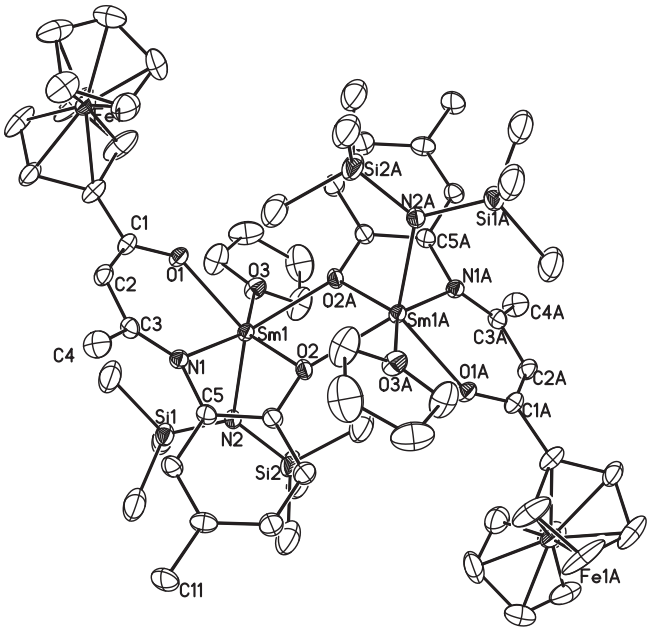

Fig. 2. ORTEP diagram of complex **2** showing atom-numbering scheme. Thermal ellipsoids are drawn at the 20% probability level. Hydrogen atoms are omitted for clarity.

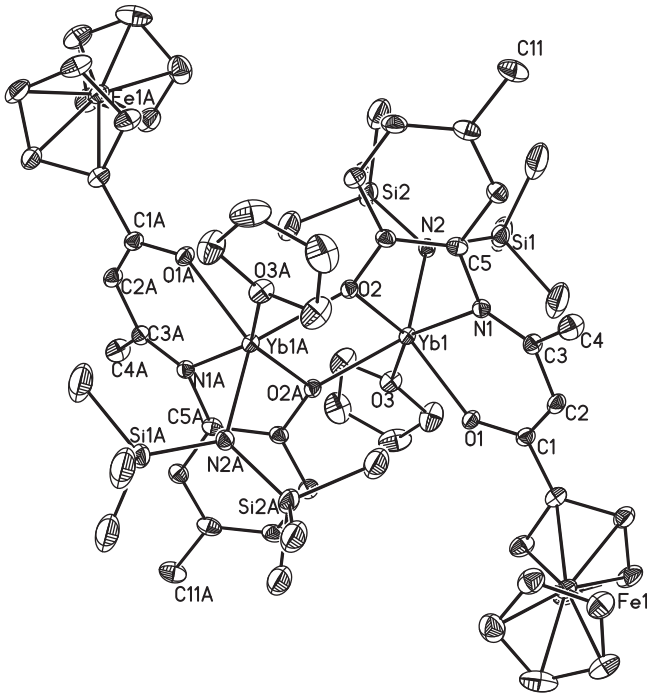

Fig. 3. ORTEP diagram of complex **4** showing atom-numbering scheme. Thermal ellipsoids are drawn at the 20% probability level. Hydrogen atoms are omitted for clarity.

structures. Intensity data were collected with a Rigaku Mercury CCD area detector in ω scan mode using Mo Kα radiation (λ = 0.71070 Å). The diffracted intensities were corrected for Lorentz polarization effects and empirical absorption corrections. Details of the intensity data collection and crystal data are given in Table 1.

The structures were solved by direct methods and refined by full-matrix least-squares procedures based on $|F|^2$. All the non-hydrogen atoms were refined anisotropically. The hydrogen atoms in these complexes were all generated geometrically, assigned appropriate isotropic thermal parameters, and allowed to ride on their parent carbon atoms. All the H atoms were held stationary and included in the structure factor calculation in the final stage of full-matrix least-squares refinement. The structures were solved and refined using SHELEXL-97.

2.9. Polymerization of L-lactide

The procedures for the polymerization of L-lactide initiated by complexes **1**–**5** were similar, and a typical polymerization procedure is given below. A 50 mL Schlenk flask, equipped with a magnetic stirring bar, was charged with the desired amount of L-lactide and toluene. The contents of the flask were then stirred at 70 °C until the L-lactide was dissolved, and then a solution of the initiator in toluene was added to this solution by syringe. The mixture was stirred vigorously at 70 °C for the desired time, during which time an increase in the viscosity was observed. The reaction mixture was quenched by the addition of methanol and then poured into methanol to precipitate the polymer, which was dried under vacuum and weighed.

3. Results and discussion

Ferrocenoylacetone was prepared by the reaction of acetylferrocene with ethyl acetate according to the literature method [16]. The reaction of ferrocenoylacetone with 1 equivalent of 2-amino-4-methyl-phenol in absolute ethanol, after workup, gave the *N*-aryloxo-functionalized β-ketoimine $FcCOCH_2C(Me)N(2\text{-}HO\text{-}5\text{-}Me\text{-}C_6H_3)$ (LH_2, Fc = ferrocenyl) in a high isolated yield, as shown in Scheme 1, which was identified by elemental analysis and ^1H NMR spectroscopy.

It was found that amine elimination reactions of lanthanide amides with 1 equivalent of LH_2 in THF is a convenient method for the synthesis of lanthanide amides stabilized by the N-aryloxo-functionalized β-ketoiminate ligand. When a THF solution of $Ln[N(TMS)_2]_3(\mu\text{-}Cl)Li(THF)_3$ was added to a suspension of LH_2 in THF in a 1:1 molar ratio at room temperature, the color of the solution changed to dark-red, and precipitate formed gradually. After workup, microcrystals of the final products $[LLnN(SiMe_3)_2(THF)]_2$ [Ln = Nd (**1**), Sm (**2**), Er (**3**), Yb (**4**), Y (**5**)] were obtained in 70–84% isolated yields as summarized in Scheme 2.

The compositions of complexes **1**–**5** were established by elemental analysis, ^1H NMR spectroscopy in the case of complex **5** and molecular structure determination of complexes **1**, **2**, and **4**. All of these complexes are extremely sensitive to air and moisture. The crystals turn to powder immediately when they are exposed to air.

Table 2
Selected bond lengths (Å) and bond angles (°) for complexes 1, 2, and 4.

complex	1	2	4
Bond length			
Ln(1)–O(1)	2.271(4)	2.235(4)	2.158(3)
Ln(1)–O(2)	2.381(4)	2.357(5)	2.267(3)
Ln(1)–O(2A)	2.372(4)	2.328(5)	2.243(3)
Ln(1)–O(3)	2.542(5)	2.501(6)	2.402(3)
Ln(1)–N(1)	2.515(5)	2.481(6)	2.384(4)
Ln(1)–N(2)	2.337(5)	2.320(5)	2.226(4)
Bond angle			
N(1)–Ln(1)–O(2)	66.25(15)	67.09(17)	69.02(12)
O(2)–Ln(1)–O(2A)	67.63(16)	67.4(2)	68.28(13)
O(2A)–Ln(1)–O(3)	81.25(16)	81.07(18)	80.28(12)
O(3)–Ln(1)–N(1)	148.44(16)	149.26(18)	149.87(13)
N(2)–Ln(1)–O(1)	125.98(17)	125.62(19)	124.60(14)
O(1)–Ln(1)–N(1)	74.02(15)	75.06(18)	77.62(12)

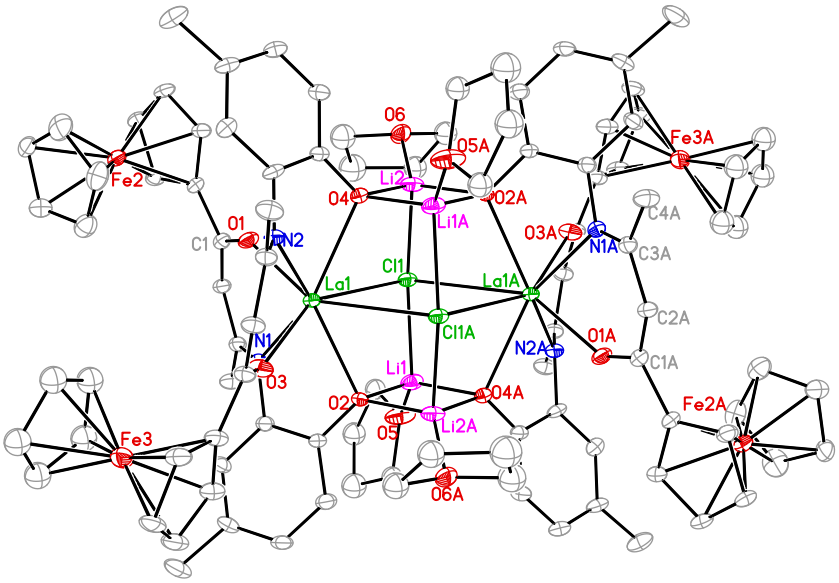

Fig. 4. ORTEP diagram of complex **6** showing atom-numbering scheme. Thermal ellipsoids are drawn at the 20% probability level. Hydrogen atoms are omitted for clarity.

All of these complexes are soluble in THF, and slightly soluble in DME and toluene.

However, reaction of LH_2 with $La[N(TMS)_2]_3(\mu\text{-}Cl)Li(THF)_3$ in a 1:1 molar ratio in THF at room temperature, after workup, gave the unexpected lanthanum-lithium bimetallic cluster $[L_2La\{\mu\text{-}Li(THF)\}_2(\mu\text{-}Cl)]_2$ (**6**), instead of the desired lanthanum amido complex $[LLaN(SiMe_3)_2(THF)]_2$ as shown in Scheme 3, which was characterized by elemental analysis, IR spectroscopy and crystal structure determination. The difference in the outcome of the amine elimination reactions is supposed to reflect the difference in the ionic radii of the lanthanide metals.

The molecular structures of complexes **1**, **2**, and **4** are shown in Figs. 1–3, and their selected bond lengths and bond angles are listed in Table 2. These complexes are isomorphous, and have centrosymmetric dimeric structures containing an Ln_2O_2 core. These lanthanide amido complexes possess bridging phenoxo oxygen atoms, which is similar to those found in the N-aryloxo-functionalized β-ketoiminate rare-earth metal chlorides and aryloxides [15]. The metal centers in these complexes are six-coordinated with two oxygen atoms and one nitrogen atom from one β-ketoiminate ligand, one nitrogen atom from the amido group, one oxygen atom from one THF molecule, and one oxygen atom from another β-ketoiminate ligand. Each of the metal centers has a highly distorted octahedral coordination geometry, which is similar to those observed in β-ketoiminate rare-earth metal aryloxides [15].

In complex **1**, the terminal Nd–O(alkoxo) bond length of 2.271 (4) Å compares well with the corresponding bond length in neodymium β-ketoiminate complex $[L'Nd(OAr)(THF)]_2$ (2.260(5) Å) (L' = OC(Me)CHC(Me)N(2–O–5–Me–C_6H_3), ArO = O–2,6–Bu^t_2–4–Me–C_6H_3) [15], but slightly smaller than that in $Nd_2[\{OC(Bu^t)CHC(Bu^t)N\}_2(CH_2)_3]_3$ (2.304(3) Å) [19]. The average Nd–O(Ar) bond length of 2.376(5) Å is comparable with the corresponding value in $[L'Nd(OAr)(THF)]_2$ (2.371(5) Å) [15]. The Nd–N(amido) bond length of 2.337(5) Å is comparable with those values in β-ketoiminato samarium and erbium amido complexes when the difference in ionic radii is considered [20]. The bond lengths of Ln–O and Ln–N in complexes **2** and **4** are comparable with the corresponding bond lengths in complex **1** when the difference in ionic radii is considered.

The ORTEP diagram of complex **6** is shown in Fig. 4, and its selected bond parameters are listed in Table 3. Complex **6** has a centrosymmetric structure that consists of four β-ketoiminato ligands, two lanthanum atoms, four lithium atoms, two chlorine atoms and four THF molecules. The molecule can be regarded as a dimer in which two $[L_2LaLi(THF)]$ moieties are connected by two

Table 3
Selected bond lengths (Å) and bond angles (°) for complex 6.

Bond lengths(Å)			
La(1)–O(1)	2.329(5)	La(1)–N(2)	2.614(6)
La(1)–O(3)	2.338(6)	La(1)–N(1)	2.619(6)
La(1)–O(2)	2.543(5)	La(1)–Cl(1A)	3.115(2)
La(1)–O(4)	2.549(5)	La(1)–Cl(1)	3.116(2)
Li(1)–Cl(1)	2.37(1)	Li(1)–O(2)	1.94(2)
Li(1)–O(4A)	1.92(1)	Li(1)–O(5)	1.88(1)
Bond angles(°)			
O(1)–La(1)–O(3)	114.2(2)	N(2)–La(1)–N(1)	133.9(2)
O(3)–La(1)–O(2)	79.33(18)	O(1)–La(1)–Cl(1)	89.24(16)
O(1)–La(1)–O(4)	78.41(17)	O(2)–La(1)–Cl(1)	70.26(12)
O(2)–La(1)–O(4)	130.49(17)	O(4)–La(1)–Cl(1)	70.76(12)
O(1)–La(1)–N(2)	86.59(18)	Cl(1A)–La(1)–Cl(1)	74.48(5)
O(3)–La(1)–N(2)	70.30(18)	La(1)–Cl(1)–La(1A)	105.52(5)
O(4)–La(1)–N(2)	63.24(19)	Li(1)–O(2)–Li(2A)	85.0(7)
O(1)–La(1)–N(1)	69.78(18)	Li(1)–O(4A)–Li(2A)	85.7(7)
O(3)–La(1)–N(1)	83.84(18)	O(4A)–Li(1)–O(2)	94.4(6)
O(2)–La(1)–N(1)	63.74(17)	Li(1)–Cl(1)–Li(2)	151.8(5)

Table 4
Polymerization of L-lactide initiated by complexes 1–5. [a]

Entry	Initiator	$[M]_0/[I]_0$ [b]	Solvent	T_p(oC)	t(h)	Yield%[c]	Mn[d](10^4)	PDI
1	**1**	100	Tol	70	4 h	100	6.72	1.53
2	**1**	200	Tol	70	4 h	100	5.87	1.68
3	**1**	300	Tol	70	4 h	100	7.56	1.86
4	**1**	400	Tol	70	5 h	35	1.12	1.39
5	**2**	200	Tol	70	4 h	93	3.05	1.78
6	**2**	300	Tol	70	5 h	50	1.32	1.46
7	**3**	200	Tol	70	4 h	78	2.76	1.65
8	**4**	100	Tol	70	4 h	72	2.35	1.58
9	**5**	200	Tol	70	4 h	42	1.07	1.39

[a] Polymerization conditions: Toluene as solvent, $V_{sol}/V_{[M]} = 1{:}1$.
[b] $[M]_0/[I]_0$ = [monomer]/[initiator].
[c] Yield: weight of polymer obtained/weight of monomer used.
[d] Measured by GPC calibrated with standard polystyrene samples.

(THF)LiCl moieties. The phenolate oxygen atoms and the chlorine atoms act as bridges, and adopt μ_3- and μ_4-bridging coordination modes, respectively. Each of the phenolate oxygen atoms is coordinated to one lanthanum atom and two lithium atoms, and each of the chlorine atoms is coordinated to two lanthanum atoms and two lithium atoms to form a three-decker cluster. The upper and the bottom are same, and contain the Li_2O_2 core. Two lithium atoms and two oxygen atoms are coplanar with the sum of the O–Li–O bond angles of 360.1(7)°. The middle consists of two lanthanum atoms and two chlorine atoms, which are also coplanar. The oxygen and nitrogen atoms of the two β-ketoiminato ligands are coordinated to one lanthanum atom, which is different from those in complexes **1**, **2** and **4**, and can be attributed to the large ionic radius of the lanthanum metal ion. Each lanthanum atom is eight-coordinate with four oxygen atoms and two nitrogen atoms from two β-ketoiminato ligands, and two chlorine atoms to form a distorted bicapped trigonal prism, in which the capping atoms are the chlorine atoms. The overall coordination geometry around the lanthanum atom is quite different from those observed in complexes **1**, **2** and **4**. Each lithium atom is coordinated to two oxygen atoms from two β-ketoiminato ligands, one chlorine atom and one oxygen atom from a THF molecule to form a distorted tetrahedron.

The average La–O(alkoxo) bond length of 2.333(6) Å in complex **6** is slightly larger than the terminal La–O(Ar) bond lengths in bridged bis(phenolate) lanthanum complexes [ONOO]La[$N(SiMe_2H)_2$](THF) [ONOO = $MeOCH_2CH_2N\{CH_2–(2–O–C_6H_2–Bu^t_2–3,5)\}_2$] [2.272(3) Å] [21], and (MBMP)La(THF)(μ-MBMP)$_2$La(THF)$_2$ [MBMP = 2,2′–CH_2–(1–O–C_6H_2–Me–4–Bu^t–6)$_2$] [2.286(4) Å] [22]. The average bridging La–O(Ar) bond length is, as expected, somewhat larger at 2.546(5) Å, which is also apparently larger than the bridging La–O(Ar) bond length in (THF)La(O–2,6–$Pr^i_2C_6H_3$)$_2$(μ–O–2,6–$Pr^i_2C_6H_3$)$_2$M(THF)$_2$ (M = Li, Na; 2.453(4) Å) [23], and the bridging Ln–O(Ar) bond length in complexes **1**, **2**, and **4** even when the difference in ionic radii is considered, indicating the increase of steric congestion around the lanthanum metal. The Li1–O2 and Li2A–O2 bond lengths are 1.94(2) and 1.92(1) Å, respectively, which indicated that the phenolate group is nearly symmetrically coordinated to two lithium atoms. The average Li–O(Ar) bond length of 1.93(1) Å is slightly shorter than those average Li–O(Ar) bond lengths reported for the bridged bis(phenolate) lithium complexes [24,25].

The catalytic behavior of the lanthanide amido complexes **1**–**5** for the ring-opening polymerization of L-lactide was examined, and the preliminary results are summarized in Table 4. It can be seen that these lanthanide amides can initiate the ring-opening polymerization of L-lactide with moderate activity, giving the resultant polymers with high molecular weights and relatively broad molecular weight distributions. However, the activity of these amide complexes is lower than that of the N-aryloxo-functionalized β-ketoiminate lanthanide aryloxides. For example, the neodymium aryloxide can completely polymerize 400 equivalents of L-lactide at 70 °C in 4 h [15], whereas complex **1** gave the yield of 35% in 5 h under the same polymerization conditions (Entry 4). A possible explanation is that the silylamide group is less nucleophilic than aryloxo group, which caused slow initiation [26]. As in the β-ketoiminate lanthanide amido systems [27,28], the central metal ion has a profound effect on the catalytic activity. The catalytic activity decreased dramatically with the decrease of the ionic radii, and the neodymium amido complex showed the highest activity among complexes **1**–**5**.

In summary, we have successfully synthesized a series of lanthanide metal complexes stabilized by a ferrocene-containing dianionic N-aryloxo-functionalized β-ketoiminate ligand, and characterized some of their structural features by X-ray diffraction studies. The ionic radii have a significant effect on the outcome of the amine elimination reactions of the β-ketoimine with lanthanide amides, and a novel lanthanum-lithium heterobimetallic cluster stabilized by this ligand was isolated.

Acknowledgment

Financial support from the National Natural Science Foundation of China (Grants 20771078, 20972108 and 20632040), the Major Basic Research Project of the Natural Science Foundation of the Jiangsu Higher Education Institutions (Project 07KJA15014), and the Qing Lan Project is gratefully acknowledged.

Appendix A. Supplementary data

CCDC 773983–773986 contain the supplementary crystallographic data for complexes **1**, **2**, **4** and **6**. These data can be obtained free of charge via http://www.ccdc.cam.ac.uk/conts/retrieving.html, or from the Cambridge Crystallographic Data Centre, 12 Union Road, Cambridge CB2 1EZ, UK; fax: +44-1223-336033; or e-mail: deposit@ccdc.cam.ac.uk.

References

[1] E.W. Piers, D.J.H. Emslie, Coord. Chem. Rev. 233–234 (2002) 131.
[2] Z. Hou, Y. Wakatsuki, Coord. Chem. Rev. 231 (2002) 1.
[3] P.J. Bailey, S. Pace, Coord. Chem. Rev. 214 (2001) 91.
[4] F.T. Edelmann, Chem. Soc. Rev. 38 (2009) 2253.
[5] L. Bourget-Merle, M.F. Lappert, J.R. Severn, Chem. Rev. 102 (2002) 3031.
[6] X.C. Zhu, J.X. Fan, Y.J. Wu, S.W. Wang, L.J. Zhang, G.S. Yang, Y. Wei, C.W. Yin, H. Zhu, S.H. Wu, H.T. Zhang, Organometallics 28 (2009) 3882.
[7] B.D. Fahlman, Curr. Org. Chem. 10 (2006) 1021.
[8] T. Punniyamurthy, S. Velusamy, J. Iqbal, Chem. Rev. 105 (2005) 2329.
[9] L.M. Tang, Y.G. Li, W.P. Ye, Y.S. Li, J. Polym, Sci. Part A: Polym. Chem. 44 (2006) 5846.
[10] H.Y. Wang, J. Zhang, X. Meng, G.X. Jin, J. Organomet. Chem. 691 (2006) 1275.
[11] H.Y. Tang, H.Y. Chen, J.H. Huang, C.C. Lin, Macromolecules 40 (2007) 8855.
[12] S.A. Schuetz, E.A. Bowman, C.M. Silvernail, V.W. Day, J.A. Belot, J. Organomet. Chem. 690 (2005) 1011.
[13] S.A. Schuetz, C.M. Silvernail, C.D. Incarvito, A.L. Rheingold, J.L. Clark, V.W. Day, J.A. Belot, Inorg. Chem. 43 (2004) 6203.
[14] S.A. Schuetz, V.W. Day, A.L. Rheingold, J.A. Belot, Dalton Trans. (2003) 4303.
[15] H.M. Peng, Z.Q. Zhang, R.P. Qi, Y.M. Yao, Y. Zhang, Q. Shen, Y.X. Cheng, Inorg. Chem. 47 (2008) 9828.
[16] Y.C. Shi, H.M. Yang, W.B. Shen, C.G. Yan, X.Y. Hu, Polyhedron 23 (2004) 15.
[17] S.L. Zhou, S.W. Wang, G.S. Yang, X.Y. Liu, E.H. Sheng, K.H. Zhang, L. Cheng, Z.X. Huang, Polyhedron 22 (2003) 1019.
[18] J.L. Atwood, W.E. Hunter, A.L. Wayda, W.J. Evans, Inorg. Chem. 20 (1981) 4115.
[19] W.S. Rees Jr., O. Just, S.L. Castro, J.S. Matthews, Inorg. Chem. 39 (2000) 3736.
[20] S.A. Schuetz, V.W. Day, R.D. Sommer, A.L. Rheingold, J.A. Belot, Inorg. Chem. 40 (2001) 5292.
[21] C.X. Cai, A. Amgoune, C.W. Lehmann, J.F. Carpentier, Chem. Commun. (2004) 330.
[22] R.P. Qi, B. Liu, X.P. Xu, Z.J. Yang, Y.M. Yao, Y. Zhang, Q. Shen, Dalton Trans. (2008) 5016.
[23] D.L. Clark, R.L. Vincent-Hollis, B.L. Scott, J.G. Watkin, Inorg. Chem. 35 (1996) 667.
[24] B.T. Ko, C.C. Lin, J. Am, Chem. Soc. 123 (2001) 7973.
[25] C.A. Huang, C.T. Chen, Dalton Trans. (2007) 5561.
[26] H.Y. Ma, J. Okuda, Macromolecules 38 (2005) 2665.
[27] X.Z. Han, L.L. Wu, Y.M. Yao, Y. Zhang, Q. Shen, Chin. Sci. Bull. 54 (2009) 3795.
[28] B. Xu, X.Z. Han, Y.M. Yao, Y. Zhang, Q. Shen, Chin. J. Chem. 28 (2010) 1013.